

中国激光

激光熔覆碳纳米管增强高熵合金涂层及耐腐蚀性能

韩冰^{1,2*}, 陈曦³, 姜梦³, 陈文龙⁴, 张东东⁵, 曹立超², 张俊爽¹, 滕宪斌¹, 陈彦宾³

¹广州航海学院轮机工程学院, 广东 广州 510725;

²广东省科学院智能制造研究所, 广东 广州 510070;

³哈尔滨工业大学先进焊接与连接国家重点实验室, 黑龙江 哈尔滨 150001;

⁴广东省科学院工业分析检测中心, 广东 广州 510650;

⁵攀枝花学院钒钛学院, 四川 攀枝花 617000

摘要 通过机械混合方法解决了碳纳米管(CNTs)在CoCrFeNi高熵合金粉体表面的团聚问题,采用激光熔覆方法在304不锈钢基板上制备了CoCrFeNi-CNTs涂层,碳纳米管优化质量分数为1.0%,研究了涂层微观组织、显微硬度及抗中性盐雾腐蚀性能。结果表明:涂层的晶粒为单一的面心立方(FCC)结构,按照晶粒形态可以分为平面晶、胞状枝晶、柱状枝晶、等轴晶,晶界上形成了M₇C₃型碳化物共晶相,未分解碳纳米管弥散分布在晶粒内,Si/C类夹杂物来自于熔化的基板材料。涂层内硬度分布较均匀,由于碳纳米管和M₇C₃碳化物的第二相强化作用,硬度水平可以比CoCrFeNi涂层提高70 HV以上。经中性盐雾腐蚀269 h后,点蚀仅发生在脱落的Si/C类夹杂物周围区域,而在晶粒及晶界内其他区域均未发现腐蚀现象,因此,严格限制Si/C类夹杂物进入涂层将进一步改善复合涂层的抗中性盐雾腐蚀性能。

关键词 激光技术; 高熵合金; 硬度; 中性盐雾腐蚀

中图分类号 TG146.4 文献标志码 A

DOI: 10.3788/CJL230737

1 引言

自Yeh等^[1-2]提出一种全新的合金设计思想以来,高熵合金因其出色的力学性能及抗腐蚀性能,受到了学术界和工业界人士的广泛关注^[3-6]。等原子比的CoCrFeNi高熵合金为面心立方(FCC)晶体结构^[7-8],具有优异的低温力学性能^[9],已经成为研究CoCrFeNiMn^[10]、CoCrFeNiCu^[11]、CoCrFeNiTi^[12]等新型高熵合金的重要基础。然而,CoCrFeNi高熵合金的室温力学性能并不突出,严重限制了其在表面强化领域的应用潜力^[13]。

近年来,碳的同素异构材料(如碳纳米管、石墨、石墨烯等)已经被广泛用于强化高熵合金涂层的研究^[14-16]。Medina等^[17]将石墨靶材作为碳源,采用磁控共溅射技术制备出碳含量可调的CoCrFeMnNiC_x高熵合金薄膜,测试发现,当碳原子数分数(x)增加到11%时,薄膜的纳米压痕硬度提高到16 GPa,大幅高于无碳薄膜的8 GPa水平,耐腐蚀性能也得到进一步改善。Xiao等^[18]以石墨烯作为碳源,采用等离子体烧结技术制备出不同碳含量的CoCrFeMnNiC_x高熵合金块体,测试发

现,当碳原子数分数增加到10.7%时,合金的显微硬度由327.8 HV大幅提高到566.4 HV,而磨损速率从 $6.5 \times 10^{-5} \text{ mm}^3/(\text{N} \cdot \text{m})$ 下降到 $0.47 \times 10^{-5} \text{ mm}^3/(\text{N} \cdot \text{m})$ 。Singh等^[19]以碳纳米管作为碳源,采用等离子体烧结技术制备出不同碳含量的FeCoCrNiCuC_x高熵合金块体,测试发现,当碳原子数分数增加到9.0%时,合金的腐蚀速率比之前减小了88.6%,继续增加碳含量则腐蚀速率又会增大。显然,采用等离子体烧结技术能够制备碳掺杂高熵合金块体,但难以实现基材上涂层的快速制备。磁控溅射技术虽然可以制备碳掺杂高熵合金涂层,但涂层厚度较薄,仍难以满足机械零部件在恶劣环境下的服役要求。

近年来,激光熔覆技术已经被广泛应用于合金涂层的快速制备。得益于激光束能量密度高的特点,利用该技术能够在熔池快速凝固过程中生成细小的晶粒组织,有助于提高合金涂层的力学性能^[20-22]。研究人员已经尝试在激光熔覆CoCrFeNi系高熵合金涂层中添加适量Al、Mo、Si、B、Ti、Mn等元素以改善涂层的组织及力学性能^[23-26]。Chen等^[27]通过在激光熔覆CoCrFeNi高熵合金涂层中周期地添加适量Al元素,

收稿日期: 2023-04-17; 修回日期: 2023-05-20; 录用日期: 2023-05-30; 网络首发日期: 2023-07-04

基金项目: 国家自然科学基金(52105326)、广州市基础与应用基础研究项目(202102020725)、广东省科学院“千名博士(后)计划”引进专项(2020GDASYL-20200103125)

通信作者: *dabingzhenniu@163.com

成功制备出 FCC 和体心立方(BCC)双相结构复合涂层,涂层的显微硬度得到改善。Li 等^[28]通过在激光熔覆 CoCrFeNi 高熵合金涂层中添加适量 Ti 元素,在涂层基体中原位生成了 BCC 结构晶间析出相和弥散分布的 TiO_2 金属间化合物,涂层的显微硬度得到改善。但目前通过在激光熔覆 CoCrFeNi 高熵合金涂层中添加适当碳纳米管来实现涂层组织相变并改善显微硬度水平的研究仍然不足,针对激光熔覆 CoCrFeNi-CNTs 复合涂层的中性盐雾腐蚀行为研究依然较少。本文采用机械混合法代替高能球磨法,尝试解决碳纳米管的团聚问题,成功制备出 CoCrFeNi-CNTs 复合粉末原材料,最终通过激光熔覆技术成功制备出 CoCrFeNi-CNTs 高熵合金复合涂层,系统研究了新型高熵合金复合涂层的宏微观组织特征、显微硬度分布及其在中性盐雾条件下的腐蚀行为,为该类涂层未来的工业应用提供了参考。

2 试验材料及方法

激光熔覆试验采用的基板材料为 304 不锈钢,尺寸为 $200\text{ mm} \times 200\text{ mm} \times 9\text{ mm}$,试验前使用砂纸和丙酮清理表面。将质量分数高于 99.5% 的 Co、Cr、Fe、Ni 按等物质的量混合,利用惰性气体雾化技术制备得到 CoCrFeNi 高熵合金粉末,以该粉末作为涂层基体材料,粒度范围为 $45\sim105\text{ }\mu\text{m}$,实际测量的成分如表 1

所示。

表 1 高熵合金粉末实际测量成分

Table 1 Measured components of high-entropy alloy powder

Raw powder	Mass fraction / %			
	Co	Cr	Fe	Ni
CoCrFeNi	26.23	23.36	25.28	Bal.

以多壁的碳纳米管(CNTs)作为碳源,其最外层碳管直径范围为 $4\sim6\text{ nm}$,长度范围为 $0.5\sim2.0\text{ }\mu\text{m}$ 。碳纳米管属于纤维状一维纳米材料,表现出明显的强团聚效应,而且碳纳米管容易纠缠粘结在一起,因此碳纳米管在粉末表面的团聚问题难以解决^[29-30]。在不使用磨球的情况下,机械混合方法能够大幅地减弱碳纳米管与 CoCrFeNi 粉体发生碰撞时产生的能量、热量和形变问题,碳纳米管能够充分地与 CoCrFeNi 粉体表面发生摩擦而逐渐被剥离,从而碳纳米管在 CoCrFeNi 粉体表面的团聚问题得到解决。因此,不使用磨球是实现这一过程的关键。基于以上原因,在不放入磨球的情况下,对 CoCrFeNi 粉末和碳纳米管进行机械混合,优化参数为:碳纳米管的质量分数为 1.0%,转速为 240 r/min,混合时间为 10 h,混合后将粉末置于干燥箱内 $70\text{ }^\circ\text{C}$ 下烘干处理 4 h,罐内通入氩气防止粉末高温氧化。机械混合前后的 CoCrFeNi 粉末和碳纳米管形貌如图 1 所示。

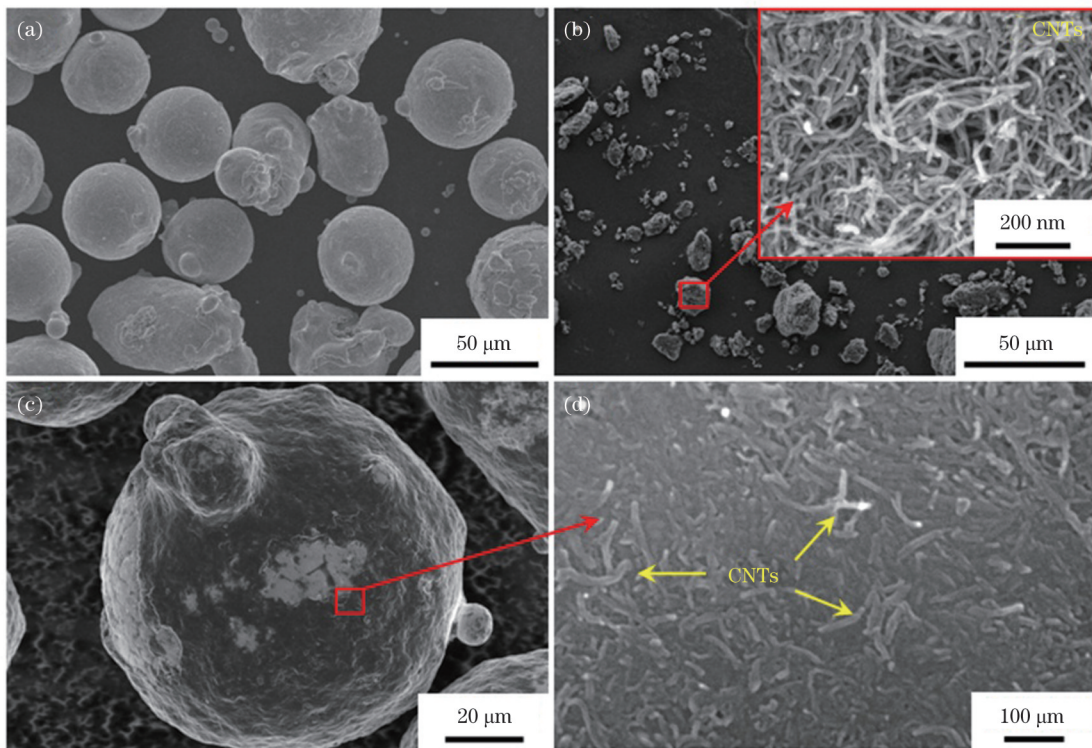


图 1 机械混合前后 CoCrFeNi 粉末和碳纳米管的显微形貌。(a)CoCrFeNi 粉末;(b)CNT 粉末;(c)CoCrFeNi-CNTs 粉末;(d)图 1 (c)局部放大

Fig. 1 Micromorphologies of CoCrFeNi powder and CNTs before and after mechanical mixing. (a) CoCrFeNi raw powder; (b) CNT raw powder; (c) CoCrFeNi-CNTs powder; (d) local magnification of Fig. 1 (c)

采用主要由光纤激光器、六轴工业机器人、送粉器组成的平台进行激光熔覆试验。为了减小 304 不锈钢基板元素对涂层化学成分的不利影响, 设定熔覆沉积 14 层金属, 采用交替扫描策略, 每层扫描路径旋转

90°, 氩气保护, 激光熔覆制备 CoCrFeNi-CNTs 复合涂层的过程及实际成形效果如图 2 所示。优化后的工艺参数如表 2 所示。

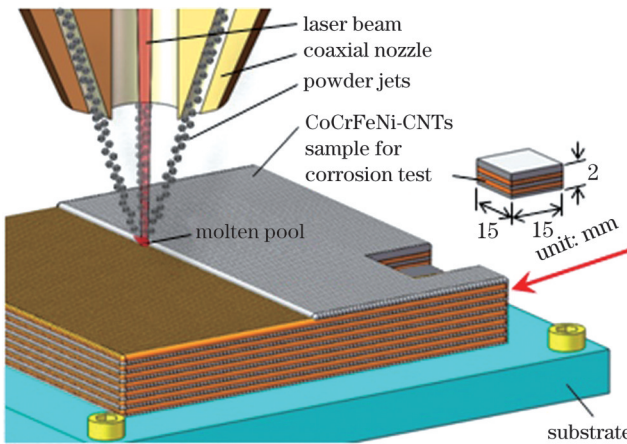


图 2 激光熔覆制备 CoCrFeNi-CNTs 复合涂层过程示意及实物图

Fig. 2 Laser cladding diagram for preparing CoCrFeNi-CNTs composite coating and physical image

表 2 激光熔覆高熵合金复合涂层的优化工艺参数

Table 2 Optimized process parameters of laser cladding CoCrFeNi high-entropy alloy composite coating

Parameter	Laser power /W	Laser scanning velocity /(mm·s ⁻¹)	Overlap rate /%	Powder feeding rate /(g·min ⁻¹)	Layer thickness /mm	Argon flow rate /(L·min ⁻¹)
Value	870	12.5	50	8.7	0.5	20

采用金相显微镜(OM)、扫描电镜(SEM)、能谱仪(EDS)对涂层截面的宏观形貌、化学成分及分布进行分析。采用 X 射线衍射仪(XRD)对涂层内的物相组成进行分析。采用透射电镜(TEM)对涂层中碳纳米管的分布特征进行观察。采用电子显微硬度仪测量涂层截面内的硬度分布, 从涂层截面的顶端向熔合线等间距进行测量, 相邻测试点间隔 0.1 mm, 载荷为 100 g, 保载时间为 15 s。采用盐雾腐蚀试验箱, 对涂层进行连续中性盐雾测试, 取样时间设定为 36、168、269 h, 采用扫描电镜对腐蚀前后涂层的微观形貌进行分析。中性盐雾测试的取样位置如图 2 所示。

3 结果与分析

3.1 复合涂层的相结构

图 3 为 CoCrFeNi 粉末原料及激光熔覆 CoCrFeNi-CNTs 复合涂层的 XRD 谱。可以看出, 虽然仅在基体中添加了质量分数为 1.0% 的碳纳米管, 在复合涂层的 XRD 谱上出现了对应碳纳米管和 M₇C₃ 碳化物相的衍射峰特征, 对应的衍射角分别为 26.6° 和 39.5°, 晶面指数分别为 (002) 和 (411)。此外, 基体的衍射峰位置与 CoCrFeNi 粉末一致, 说明基体依然由单一 FCC 结构的固溶体组成。在复合涂层 XRD 谱的最左侧还存在一些杂峰, 判断是碳纳米管受到激

光辐照而部分分解为复杂的碳同素异构体所导致的。

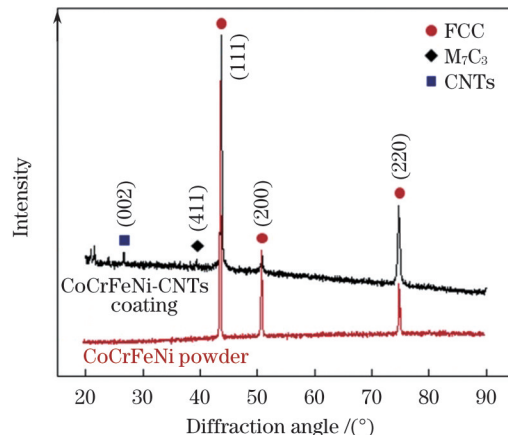


图 3 CoCrFeNi 原粉末与 CoCrFeNi-CNTs 复合涂层的 XRD 谱
Fig. 3 XRD patterns of CoCrFeNi raw powder and CoCrFeNi-CNTs composite coating

3.2 复合涂层的组织形貌

图 4 为 CoCrFeNi-CNTs 复合涂层的截面金相形貌。如图 4(a)所示, 涂层成形良好且未发现凝固裂纹的存在, 仅有少量的气孔生成, 气孔的最大直径不超过 30 μm, 其中, N 代表扫描层数, M 代表焊道数。采用交替扫描策略进行激光熔覆后, 涂层内的晶粒组织具有显著的周期分布特征。如图 4(b)所示, 在

熔池凝固过程中,将首先出现平面晶组织,而后在平面晶的基础上形成胞状晶组织。此外,在平面晶的下侧为上一沉积层残留的等轴晶组织。如图 4(c)所示,在胞状晶的基础上开始形成柱状枝晶组织。如图 4(d)所示,在柱状枝晶的基础上最终形成了等轴晶组织。单个熔池内的晶粒形态由最外侧的平面晶演变为最内侧的等轴晶,这个演变过程是由熔池中各区域成分过冷的变化导致的。在熔合线附近,由于温

度梯度较大,结晶速度又较小,故成分过冷接近于零,平面晶得到发展。随着凝固前沿向熔池中心逐渐推进,温度梯度开始减小,而结晶速度开始增加,晶粒形态先后向胞状晶、柱状枝晶和等轴晶特征转变。此外,在图 4(c)、(d)中均发现了颜色较深且形状不规则的未知物(如箭头所示),从微观形貌判断其均不属于晶内或晶间沉淀相,需要对未知物的成分及来源作进一步分析。

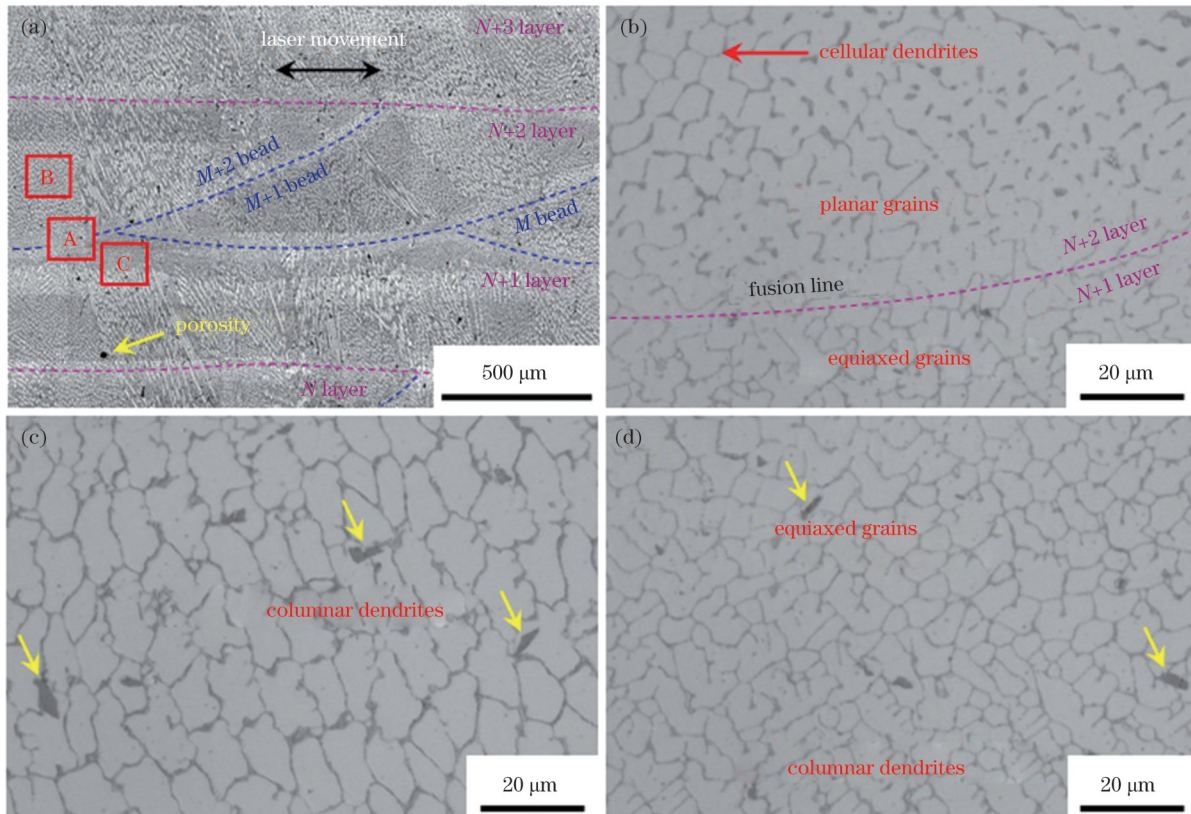


图 4 CoCrFeNi-CNTs 复合涂层的截面金相形貌。(a)涂层截面的低倍金相形貌;(b)A 区域的微观形貌;(c)B 区域的微观形貌;(d)C 区域的微观形貌

Fig. 4 Sectional metallographic morphologies of CoCrFeNi-CNTs composite coating. (a) Low magnification of metallographic morphology of coating cross section; (b) micro-morphology of region A; (c) micro-morphology of region B; (d) micro-morphology of C region

图 5 为 CoCrFeNi-CNTs 复合涂层的透射电镜显微形貌。如图 5(a)所示,沿晶界分布的 M_7C_3 碳化物具有典型的共晶结构,在晶粒内未见碳化物生成。进一步对 D 区域进行放大以分析晶间碳化物及晶内结构,如图 5(b)所示,在 M_7C_3 碳化物中出现条纹特征,可能存在层错特征,晶粒内出现弥散分布的碳纳米管形貌特征,对晶粒起到显著的第二相强化作用。 M_7C_3 碳化物内 I 区域及晶粒内 II 区域的化学成分测试结果如表 3 所示,I 区域内 Cr 元素的含量大大高于其他基体元素,说明 M_7C_3 碳化物主要由 Cr 和 C 元素构成;而 II 区域内 O 元素的含量有所增加,Cr 和 C 元素含量则大幅降低,其余四种基体元素的含量与激光熔覆前的 CoCrFeNi 原粉末基本一致。

对图 4(c)、(d)中的未知物的化学成分作进一步分析。图 6 为 CoCrFeNi-CNTs 复合涂层中未知物的扫描电镜微观形貌。未知物内 III 区域的能量谱测试结果如表 3 所示,可以看出,未知物主要由 Si 和 C 元素构成,考虑到激光熔覆试验中的 304 不锈钢基板可能曾采用 SiC 作为高效脱氧剂,判断该未知物可能为残余的 SiC 颗粒。由于 SiC 的熔点比熔池温度更高,在激光熔覆第一层粉末时就会有少量的基板金属熔入熔池,基板中残留的 SiC 颗粒被带入涂层组织中,而 SiC 的密度又显著小于熔池金属,故 SiC 颗粒会随着激光熔覆层数的增加而持续进入到涂层最顶端的更大区域内。而且,C 元素最终是以 CO 气体形式被消耗,导致残余 C 元素的含量明显低于 Si 元素。此外,Si/C 类合

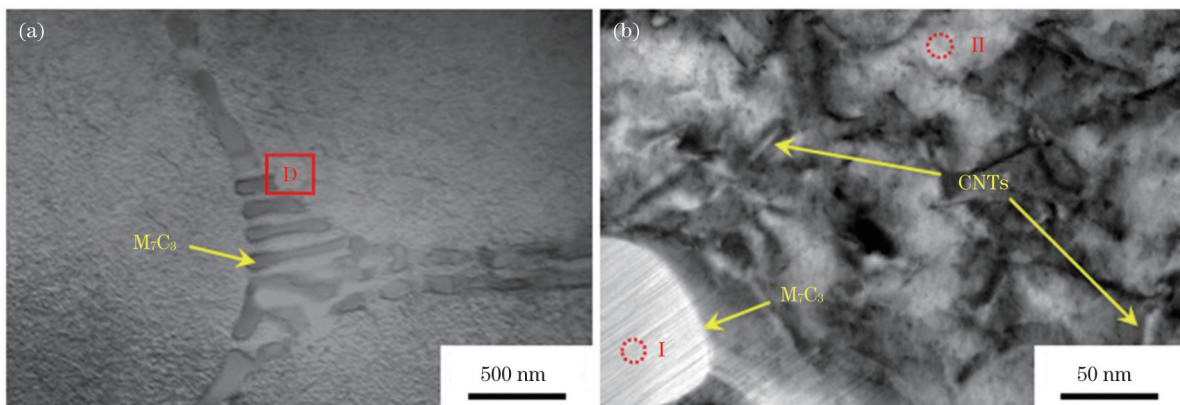
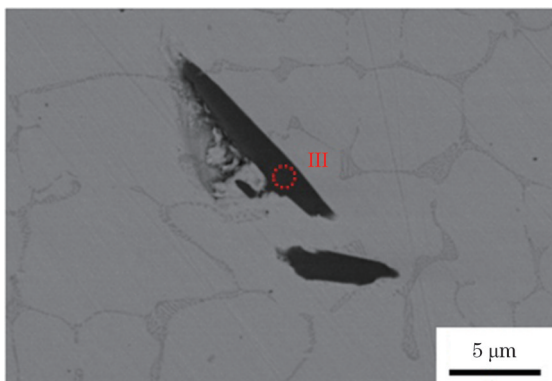


图 5 CoCrFeNi-CNTs 复合涂层的透射电镜显微形貌。(a) 晶界碳化物形貌;(b)D 区域的放大形貌

Fig. 5 TEM microstructure of CoCrFeNi-CNTs composite coating. (a) Intergranular carbide morphology; (b) enlarged morphology of D region

金作为钢中脱氧剂使用时,也同样会导致残余物中 Si 含量大大高于 C。因此,可以将该未知物命名为 Si/C 类夹杂物。

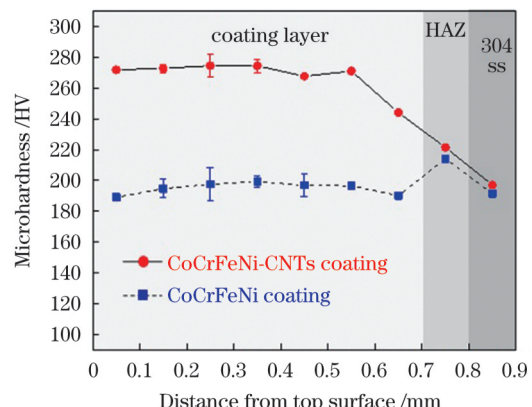
图 6 CoCrFeNi-CNTs 复合涂层中未知物的扫描电镜显微形貌
Fig. 6 SEM microstructure of unknown substances in CoCrFeNi-CNTs composite coating表 3 CoCrFeNi-CNTs 复合涂层微观区域的 EDS 测试结果
Table 3 EDS results measured at microscopic areas of CoCrFeNi-CNTs composite coating

Area	Atomic number fraction /%						
	Co	Cr	Fe	Ni	C	O	Si
I	3.99	49.23	6.63	1.22	38.93	-	-
II	23.14	23.25	25.02	23.59	3.37	1.63	-
III	-	-	-	-	27.73	-	72.27

3.3 复合涂层的硬度

图 7 为 CoCrFeNi-CNTs 和 CoCrFeNi 涂层内显微硬度分布特征的对比结果。可以看出,碳纳米管的添加使复合涂层的显微硬度提升了 70 HV 左右,说明 CoCrFeNi-CNTs 复合涂层晶界内形成的 M₇C₃ 碳化物及晶粒内弥散分布的碳纳米管结构对 CoCrFeNi 基体的显微硬度水平具有显著的第二相强化作用。此外,由于 304 不锈钢基板(SS)对邻近的涂层成分有较

的稀释作用,在靠近热影响区(HAZ)的涂层内显微硬度有所下降。在热输入作用下,热影响区内的硬度高于 304 基板母材及未添加碳纳米管的 CoCrFeNi 涂层。

图 7 CoCrFeNi-CNTs 和 CoCrFeNi 涂层内的显微硬度分布对比
Fig. 7 Comparison of microhardness distributions in CoCrFeNi-CNTs and CoCrFeNi coatings

3.4 复合涂层的盐雾腐蚀行为

图 8 为 CoCrFeNi-CNTs 复合涂层在经历不同盐雾腐蚀时长后的扫描电镜微观形貌。如图 8(a)所示,在经历 36 h 的盐雾腐蚀后,晶粒和晶界组织未见明显的腐蚀迹象,Si/C 类夹杂物特征也未见改变。如图 8(b)所示,当盐雾腐蚀时长增加到 168 h 时,晶粒和晶界处仍未见明显的腐蚀现象发生,但 Si/C 类夹杂物已经出现了部分脱落的现象。如图 8(c)、(d)所示,当盐雾腐蚀时长继续增加到 269 h 时,在 Si/C 类夹杂物脱落的区域内腐蚀反应加快进行,表现为点蚀特征,在点蚀坑周围还存在沿晶界分布的微裂纹,说明晶界处的侵蚀导致点蚀坑持续扩大。如图 8(e)、(f)所示,在腐蚀坑内及边缘处 C 和 Si 元素的含量明显高于其他区域,判断为残留的少量 Si/C 类夹杂物,说明点蚀是在脱落 Si/C 类夹杂物的区域内发生的。

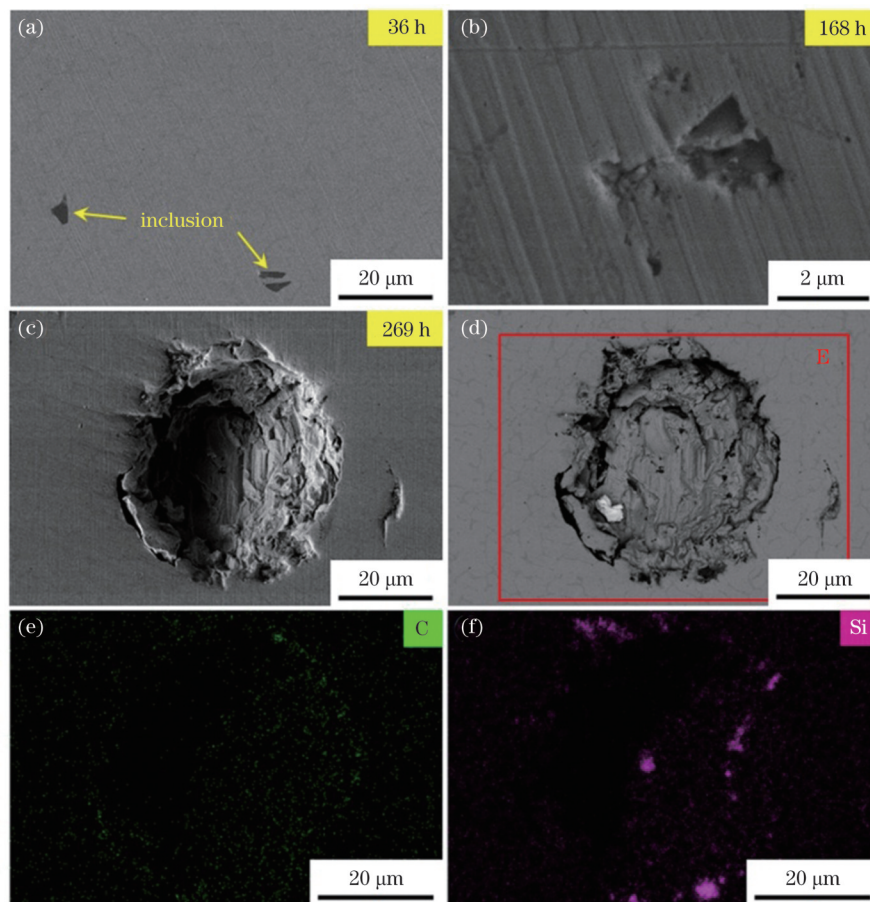


图8 不同盐雾腐蚀时长下CoCrFeNi-CNTs复合涂层的扫描电镜显微形貌。(a) 36 h;(b) 168 h;(c) 269 h(二次电子模式下成像);(d) 269 h(背散射模式下成像);(e)E区域的碳元素分布;(f)E区域的硅元素分布

Fig. 8 SEM microstructures of CoCrFeNi-CNTs composite coating under different salt spray corrosion time. (a) 36 h; (b) 168 h; (c) 269 h (imaging in secondary electron mode); (d) 269 h (imaging in backscatter mode); (e) distribution of C element in area E; (f) distribution of Si element in area E

4 结 论

在优化参数下采用机械混合方法能够实现碳纳米管在CoCrFeNi粉体表面的均匀包覆,有效解决了碳纳米管的固有团聚问题,为碳纳米管增强激光熔覆CoCrFeNi涂层的成功制备提供了支持。

CoCrFeNi-CNTs复合涂层内无裂纹缺陷生成,气孔直径小于30 μm,晶粒组织由单一FCC结构的平面晶、胞状枝晶、柱状枝晶、等轴晶组成,晶界组织由M₇C₃碳化物共晶组成,利用透射电镜发现残余碳纳米管在晶粒内弥散分布。

CoCrFeNi-CNTs复合涂层内碳化物和残余碳纳米管均具有第二相强化作用,涂层的显微硬度水平能够提高70 HV以上。

M₇C₃碳化物共晶及碳纳米管的存在并未显著降低复合涂层内晶粒及晶界的耐腐蚀性能,但被304不锈钢基板引入复合涂层内的Si/C类夹杂物会对复合涂层的耐腐蚀性能产生不利影响,点蚀现象会在脱落的Si/C类夹杂物区域内发生,晶界处的侵蚀导致点蚀坑持续扩大。

参 考 文 献

- [1] Yeh J W, Chen S K, Lin S J, et al. Nanostructured high-entropy alloys with multiple principal elements: novel alloy design concepts and outcomes[J]. Advanced Engineering Materials, 2004, 6(5): 299-303.
- [2] Yeh J W, Chang S Y, Hong Y D, et al. Anomalous decrease in X-ray diffraction intensities of Cu-Ni-Al-Co-Cr-Fe-Si alloy systems with multi-principal elements[J]. Materials Chemistry and Physics, 2007, 103(1): 41-46.
- [3] 邹朋津, 董刚, 王梁, 等. 激光熔覆制备CrNiAlCoMoB_{0.5}高熵合金涂层的组织与耐腐蚀性能研究[J]. 中国激光, 2015, 42(s1): s103003.
- [4] Zou P J, Dong G, Wang L, et al. Microstructure and corrosion resistance properties of CrNiAlCoMoB_{0.5} high entropy alloy coating prepared by laser cladding[J]. Chinese Journal of Laser, 2015, 42 (s1): s103003.
- [5] 张松, 吴臣亮, 伊俊振, 等. Fe_xCoCrAlCu/Q235激光合金化层组织及性能研究[J]. 中国激光, 2014, 41(8): 0803006.
- Zhang S, Wu C L, Yi J Z, et al. Study on microstructure and performance of a Fe_xCoCrAlCu/Q235 laser alloying coatings[J]. Chinese Journal of Lasers, 2014, 41(8): 0803006.
- [6] Su J, Raabe D, Li Z M. Hierarchical microstructure design to tune the mechanical behavior of an interstitial TRIP-TWIP high-entropy alloy[J]. Acta Materialia, 2019, 163: 40-54.
- Fan Q K, Chen C, Fan C L, et al. Ultrasonic suppression of element segregation in gas tungsten arc cladding AlCoCuFeNi high-entropy alloy coatings[J]. Surface and Coatings Technology,

- 2021, 420: 127364.
- [7] Qi Y L, Cao T H, Zong H X, et al. Enhancement of strength-ductility balance of heavy Ti and Al alloyed FeCoNiCr high-entropy alloys via boron doping[J]. Journal of Materials Science & Technology, 2021, 75: 154-163.
- [8] Feng H, Cui S Y, Chen H T, et al. A molecular dynamics investigation into deformation mechanism of nanotwinned Cu/high entropy alloy FeCoCrNi nanolaminates[J]. Surface and Coatings Technology, 2020, 401: 126325.
- [9] Gludovatz B, Hohenwarter A, Catoor D, et al. A fracture-resistant high-entropy alloy for cryogenic applications[J]. Science, 2014, 345(6201): 1153-1158.
- [10] 翁子清, 董刚, 张群莉, 等. 退火对激光熔覆 FeCrNiCoMn 高熵合金涂层组织与性能的影响[J]. 中国激光, 2014, 41(3): 0303002. Weng Z Q, Dong G, Zhang Q L, et al. Effects of annealing on microstructure and properties of FeCrNiCoMn high-entropy alloy coating prepared by laser cladding[J]. Chinese Journal of Lasers, 2014, 41(3): 0303002.
- [11] 王勇, 李明宇, 孙丽丽, 等. FeCrNiCo(Cu/Mn)高熵合金组织及腐蚀性能[J]. 中国有色金属学报, 2020, 30(1): 94-102. Wang Y, Li M Y, Sun L L, et al. Microstructure and corrosion property of FeCrNiCo(Cu/Mn) high entropy alloys[J]. The Chinese Journal of Nonferrous Metals, 2020, 30(1): 94-102.
- [12] 李萍, 庞胜娇, 赵杰, 等. CoCrFeNiTi_{0.5}高熵合金在熔融 Na₂SO₄-25%NaCl 中的腐蚀行为[J]. 中国有色金属学报, 2015, 25(2): 367-374. Li P, Pang S J, Zhao J, et al. Corrosion behavior of CoCrFeNiTi_{0.5} high entropy alloy in molten Na₂SO₄-25%NaCl[J]. The Chinese Journal of Nonferrous Metals, 2015, 25(2): 367-374.
- [13] Peng Y W, Gong J M, Christiansen T L, et al. Surface modification of CoCrFeNi high entropy alloy by low-temperature gaseous carburization[J]. Materials Letters, 2021, 283: 128896.
- [14] Bahrami A, Mohammadnejad A, Sajadi M. Microstructure and mechanical properties of spark plasma sintered AlCoFeMnNi high entropy alloy (HEA)-carbon nanotube (CNT) nanocomposite[J]. Journal of Alloys and Compounds, 2021, 862: 158577.
- [15] Chen L B, Wei R, Tang K, et al. Heavy carbon alloyed FCC-structured high entropy alloy with excellent combination of strength and ductility[J]. Materials Science and Engineering: A, 2018, 716: 150-156.
- [16] Luo T, Zhang H L, Liu R R, et al. Mechanical and damping properties of the multi-layer graphenes enhanced CrMnFeCoNi high-entropy alloy composites produced by powder metallurgy[J]. Materials Letters, 2021, 293: 129682.
- [17] Medina L Z, Tavares da Costa M V, Paschalidou E M, et al. Enhancing corrosion resistance, hardness, and crack resistance in magnetron sputtered high entropy CoCrFeMnNi coatings by adding carbon[J]. Materials & Design, 2021, 205: 109711.
- [18] Xiao J K, Tan H, Chen J, et al. Effect of carbon content on microstructure, hardness and wear resistance of CoCrFeMnNiC_x high-entropy alloys[J]. Journal of Alloys and Compounds, 2020, 847: 156533.
- [19] Singh S, Shaikh S M, Kumar M K P, et al. Microstructural homogenization and substantial improvement in corrosion resistance of mechanically alloyed FeCoCrNiCu high entropy alloys by incorporation of carbon nanotubes[J]. Materialia, 2020, 14: 100917.
- [20] 李洪波, 郭猛, 王琳, 等. H13/Ni/WC 混合粉末梯度熔覆层的激光熔覆制备及耐磨性研究[J]. 激光与光电子学进展, 2021, 58(3): 0314006. Li H B, Guo M, Wang L, et al. Laser cladding preparation and wear resistance of H13/Ni/WC hybrid powder gradient cladding layer[J]. Laser & Optoelectronics Progress, 2021, 58(3): 0314006.
- [21] 张宇鹏, 王永东, 徐刚, 等. 石墨烯对激光熔覆 Ti-C-Nb 增强 Ni 基涂层组织与性能的影响[J]. 激光与光电子学进展, 2022, 59(1): 0114002. Zhang Y P, Wang Y D, Xu G, et al. Effect of graphene on microstructure and properties of laser cladding Ti-C-Nb-reinforced Ni-based coating[J]. Laser & Optoelectronics Progress, 2022, 59(1): 0114002.
- [22] 刘昊, 高强, 满家祥, 等. 激光熔覆 CoCrFeMnNiTi_x高熵合金涂层的微观组织及性能研究[J]. 中国激光, 2022, 49(8): 0802002. Liu H, Gao Q, Man J X, et al. Microstructure and properties of CoCrFeMnNiTi_x high-entropy alloy coating by laser cladding[J]. Chinese Journal of Lasers, 2022, 49(8): 0802002.
- [23] Juan Y F, Li J, Jiang Y Q, et al. Modified criterions for phase prediction in the multi-component laser-clad coatings and investigations into microstructural evolution/wear resistance of FeCrCoNiAlMo_x laser-clad coatings[J]. Applied Surface Science, 2019, 465: 700-714.
- [24] Shu F Y, Liu S, Zhao H Y, et al. Structure and high-temperature property of amorphous composite coating synthesized by laser cladding FeCrCoNiSiB high-entropy alloy powder[J]. Journal of Alloys and Compounds, 2018, 731: 662-666.
- [25] Guo Y X, Shang X J, Liu Q B. Microstructure and properties of *in situ* TiN reinforced laser cladding CoCr₂FeNiTi_x high-entropy alloy composite coatings[J]. Surface and Coatings Technology, 2018, 344: 353-358.
- [26] Zhang H F, Yan H L, Yu H, et al. The effect of Co and Cr substitutions for Ni on mechanical properties and plastic deformation mechanism of FeMnCoCrNi high entropy alloys[J]. Journal of Materials Science & Technology, 2020, 48: 146-155.
- [27] Chen D, Guan Y J, Jin G, et al. *In-situ* synthesis of a FeCoCrNiCu/FeCoCrNiAl composite high entropy alloy coating by laser cladding [J]. Surface and Coatings Technology, 2023, 461: 129447.
- [28] Li Y Y, Liu H, Liu X H, et al. Microstructure, thermostability and tribological behavior of composite CoCrFeNiTi_x high-entropy alloy coatings fabricated by laser cladding[J]. Optik, 2023, 283: 170899.
- [29] 张家诚, 江吉彬, 黄旭, 等. 碳纳米管含量对激光熔覆镍基复合涂层组织与性能的影响[J]. 中国激光, 2022, 49(2): 0202301. Zhang J C, Jiang J B, Huang X, et al. Effect of carbon nanotubes content on microstructure and properties of laser cladded Ni-based composite coating[J]. Chinese Journal of Lasers, 2022, 49(2): 0202301.
- [30] 寿寅任, 潘卓, 曹正轩, 等. 基于碳纳米管泡沫的高效宽谱紫外辐射[J]. 光学学报, 2022, 42(11): 1134021. Shou Y R, Pan Z, Cao Z X, et al. Efficient broad spectrum extreme ultraviolet based on carbon nanotube foam[J]. Acta Optica Sinica, 2022, 42(11): 1134021.

Laser Cladding High-Entropy Alloy Coating Reinforced by Carbon Nanotubes and Its Corrosion Resistance

Han Bing^{1,2*}, Chen Xi³, Jiang Meng³, Chen Wenlong⁴, Zhang Dongdong⁵, Cao Lichao²,
Zhang Junshuang¹, Teng Xianbin¹, Chen Yanbin³

¹School of Marine Engineering, Guangzhou Maritime University, Guangzhou 510725, Guangdong, China;

²Institute of Intelligent Manufacturing, Guangdong Academy of Science, Guangzhou 510070, Guangdong, China;

³State Key Laboratory of Advanced Welding and Joining, Harbin Institute of Technology, Harbin 150001,
Heilongjiang, China;

⁴Center for Industrial Analysis and Testing, Guangdong Academy of Science, Guangzhou 510650, Guangdong, China;

⁵School of Vanadium and Titanium, Panzhihua University, Panzhihua 617000, Sichuan, China

Abstract

Objective The research of laser cladding CoCrFeNi high-entropy coating reinforced by carbon nanotubes (CNTs) is still limited. The corrosion resistance of a new CoCrFeNi-CNTs composite coating is highly necessary. However, solving the agglomeration problem of CNTs on raw powder surface is quite challenging and key in the laser cladding process of CoCrFeNi-CNTs composite coating. The microstructure and neutral salt spray corrosion resistance are highly important characteristics for studying laser cladding CoCrFeNi-CNTs composite coating.

Methods CoCrFeNi and multi-walled CNTs raw powders are mixed by mechanical mixing method without milling ball. The optimized mixing parameters are CNT mass fraction of 1.0%, rotation speed of 240 r/min, mixing time of 10 h, drying time of 4 h, and argon gas protection. The CoCrFeNi-CNTs composite coating is fabricated on a 304 stainless steel substrate using a system platform consisting of a 6-axis industrial robot, a fiber laser, a powder feeder, and an alternating strategy with 90° rotation for each layer. The optimized laser cladding parameters are laser power of 870 W, laser scanning velocity of 12.5 mm/s, overlap rate of 50%, powder feeding rate of 8.7 g/min, layer thickness of 0.5 mm, and argon gas flow rate of 20 L/min. The macrostructural characteristics of the CoCrFeNi-CNTs composite coating is observed using an optical microscope (OM). The precipitated phases are detected using an X-ray diffraction (XRD). The microstructural features of the CoCrFeNi-CNTs composite powder and CoCrFeNi-CNTs composite coating are analyzed using a scanning electron microscope (SEM). The elemental distributions of grain, intergranular carbide eutectics, and inclusion in the CoCrFeNi-CNTs composite coating are investigated using an energy dispersive spectrometry (EDS). The distribution of CNTs in the CoCrFeNi-CNTs composite coating is further observed using a transmission electron microscope (TEM). The microhardness distribution from top to fusion line in the CoCrFeNi-CNTs composite coating is tested using a digital microhardness tester under the parameters of load of 100 g, dwell time of 15 s, and test position spacing of 0.1 mm. The neutral salt spray corrosion resistance of the CoCrFeNi-CNTs composite coating is tested using a salt spray corrosion test chamber under corrosion time of 36, 168, and 269 h.

Results and Discussions The agglomeration problem of CNTs on CoCrFeNi raw powder surface is solved successfully through the mechanical mixing method [Figs. 1(c) and (d)]. The original microstructural features of CoCrFeNi raw powder and CNTs are well protected as the energy is greatly reduced without using a milling ball (Fig. 1). Then, the CoCrFeNi-CNTs composite coating with nice internal forming is prepared on 304 stainless steel by laser cladding (Fig. 2). The grains of the CoCrFeNi-CNTs composite coating exhibit a single face-centered cubic (FCC) structure (Fig. 3). According to the morphological difference, the grains can be divided into planar grain, cellular dendrite, columnar dendrite, and equiaxed grain (Fig. 4). The M₇C₃ type carbide eutectics are formed at the grain boundaries [Fig. 5(a)]. The undecomposed CNTs are dispersed within the grain [Fig. 5(b)]. The Si/C inclusion is derived from the molten substrate material [Figs. 4(c) and (d), Fig. 6, and Table 3]. The hardness distribution in the CoCrFeNi-CNTs composite coating is uniform (Fig. 7). Owing to the second phase strengthening effect of CNTs and M₇C₃ carbides, the hardness level can be increased by over 70 HV compared to that of the CoCrFeNi coating (Fig. 7). After 269 h neutral salt spray corrosion, pitting occurs only in the area around the shed Si/C inclusion, but no corrosion is found in the grain or other area within the grain boundary (Fig. 8).

Conclusions The mechanical mixing method can effectively inhibit the agglomeration tendency of the CNTs on the surface of the CoCrFeNi powder, and the microstructures of the CoCrFeNi powder and CNTs are well protected, laying the foundation for the subsequent laser cladding process. The macro- and micro-forms of the CoCrFeNi-CNTs composite coating are good and no crack is observed. The pore diameters are not over 30 μm. The CoCrFeNi-CNTs composite coating exhibits a single face-centered cubic crystal structure. The grains can be divided into planar grain, cellular dendrite, columnar dendrite, and equiaxed grain in accordance with the morphological difference. After entering the coating molten pool, the CNTs are partially cleaved to free carbon, which is distributed within the grain boundaries and grains. The solution carbon at the grain boundary forms M₇C₃ type carbide eutectics with

Cr. The other CNTs retain the original microstructure and disperse in the grain. The microhardness of the CoCrFeNi-CNTs composite coating is increased by over 70 HV by the multiple reinforcement of the intergranular M_7C_3 type carbide eutectics, in-grain CNTs, and solution carbon. The presence of M_7C_3 type carbide eutectics and CNTs will not significantly reduce the corrosion resistance of the CoCrFeNi-CNTs composite coating; however, the inclusion of Si/C in the coating from 304 stainless steel substrate will have an adverse effect on the corrosion resistance of the CoCrFeNi-CNTs composite coating. Pitting corrosion will be formed in the region of the dropped Si/C inclusion. Therefore, strictly restricting the inclusion of Si/C into the coating will further improve the corrosion resistance of the CoCrFeNi-CNTs composite coating.

Key words laser technique; high-entropy alloy; hardness; neutral salt spray corrosion